High density collimated beams of relativistic ions produced by petawatt laser pulses in plasmas

Y. Sentoku,[1] T. V. Liseikina,[2] T. Zh. Esirkepov,[3] F. Califano,[4] N. M. Naumova,[5] Y. Ueshima,[6] V. A. Vshivkov,[2] Y. Kato,[5] K. Mima,[1] K. Nishihara,[1] F. Pegoraro,[4] and S. V. Bulanov[5]

[1]*Institute of Laser Engineering, Osaka University, Osaka, Japan*

[2]*Institute of Computation Technology, SD RAS, Novosibirsk, Russia*

[3]*Moscow Institute of Physics and Technology, Dolgoprudny, Russia*

[4]*Dipartimento di Fisica, Università di Pisa and INFM, Pisa, Italy*

[5]*APRC-Kansai Research Establishment, JAERI, Kizu, Kyoto, Japan*

[6]*APRC-Kansai Research Establishment, JAERI, Neyagawa, Osaka, Japan*

(Received 23 August 1999; revised manuscript received 13 April 2000)

Under optimal interaction conditions ions can be accelerated up to relativistic energies by a petawatt laser pulse in both underdense and overdense plasmas. Two-dimensional particle in cell simulations show that the laser pulse drills a channel through an underdense plasma slab due to relativistic self-focusing. Both ions and electrons are accelerated in the head region of the channel. However, ion acceleration is more effective at the end of the slab. Here electrons from the channel expand in vacuum and are followed by the ions dragged by the Coulomb force arising from charge separation. A similar mechanism of ion acceleration occurs when a super-intense laser pulse interacts with a thin slab of overdense plasma and the pulse ponderomotive pressure moves all the electrons away from a finite-diameter spot.

PACS number(s): 52.40.Nk, 52.65.Rr

I. INTRODUCTION

It has been known for a long time that the interaction of ultraintense laser pulses with plasmas leads to the generation of fast particles, from x- and γ-ray photons to high energy ions, electrons, and positrons [1–14]. However, completely new conditions occur when the plasma is irradiated by a petawatt laser pulse. In this case ion acceleration becomes a major feature of the plasma dynamics even in the case of short pulses.

An ultrahigh intensity laser pulse in a plasma undergoes relativistic self-focusing, which leads to the channeling of the laser radiation. The dynamics of the plasma channel produced by a multiterawatt laser pulse in an underdense plasma was studied experimentally in Ref. [10]. Self-focusing and channeling of the laser pulse were reported and the dynamics of the excitation and ionization of the ambient gas was studied. A high radial ionization velocity of the surrounding gas was observed after the formation of the channel. It was attributed to fast ions propagating radially outward with respect to the channel, under the effect of the electrostatic field arising from charge separation when the electrons are expelled from the channel [15]. Following Ref. [16], this ion acceleration mechanism was called the ''Coulomb explosion.''

In Refs. [10] and [15] the ion acceleration is associated with the breaking of plasma quasineutrality when electrons are expelled from the self-focusing radiation channel in the plasma and the ions expand due to the repulsion of the non-compensated electrical charge. The typical energy of the fast ions was calculated by balancing the force due to charge separation $[\Delta\varphi = 4\pi e(n_i - n_e)]$ with the ponderomotive force of the laser radiation on the electrons $[\mathbf{F} = -mc^2\boldsymbol{\nabla}_\perp(1+a_e^2)^{1/2}]$. Here $a_e = eE/m\omega c$. Thus the ion energy is proportional to the ponderomotive potential and scales as $mc^2 a_e$ for $a_e \gg 1$. In these estimates it is implied that the laser-plasma interaction is adiabatic on the electron time scale and that the response of ions is much slower.

In the regime of nonadiabatic interaction of the laser pulse with the plasma, the ion acceleration is more effective and the ion energy scales as $mc^2 a_e^2$. To reach such a regime of effective ion acceleration laser pulses are required in the petawatt power range, as we discuss below. Moreover, two-dimensional (2D) particle in cell (PIC) simulations [17] indicate that additional mechanisms of ion acceleration are at work and that ions are accelerated both in the radial and in the forward directions.

In the case of an overdense plasma the role of the channel is taken by the hole bored by the laser pulse [18]. In the case of a thin foil [3,19], one-dimensional (1D) PIC simulations have shown that ions are accelerated in the forward direction. These latter results were obtained within the framework of a planar model which is valid as long as the transverse size of the laser pulse is much larger than the acceleration length. However, such planar models overestimate the ion acceleration since the electrostatic potential grows indefinitely as the size of the plasma cloud increases. Therefore higher dimensional simulations are needed. Such simulations are also needed in the case of ultraintense laser pulses in near-critical density plasmas and in overdense plasmas, as these pulses are subject to relativistic self-focusing, the description of which requires at least 2D PIC simulations.

Simple analytical estimates of the energy that the ions can acquire, as a function of the pulse amplitude and shape and of the plasma parameters, can be obtained only with 1D models (with planar, cylindrical, or spherical symmetry). Nevertheless, these estimates are useful in multidimensional PIC simulations as the starting point in order to identify the optimal regimes for ion acceleration. In the following we show that the scaling of the ion energy with the pulse intensity can be optimized by considering regimes where the interaction between the laser pulse and the plasma is nonadia-

batic. Such a regime is realized, e.g., when the pulse is sufficiently short or when a long pulse develops a sharp front [20] due to its nonlinear evolution.

An electron interacting with a plane electromagnetic wave acquires an energy equal to $\mathcal{E}_e = mc^2 a_e^2/2 = Mc^2 a_h^2/2$ where

$$a_h \equiv \frac{eE}{\sqrt{mM}\,\omega c} \equiv \sqrt{\frac{m}{M}}\, a_e , \tag{1}$$

and M/m is the ion to electron mass ratio. For intensities of the order of $I \approx 2\times 10^{21}$ W/cm^2, corresponding to laser pulses with powers in the petawatt range, the value of the dimensionless amplitude is of order 1. This means that the electrons in the wave field become as heavy as ions. In an underdense plasma a short laser pulse generates a plasma wake wave with amplitude $\varphi = \mathcal{E}_e/e$, where φ is the electrostatic potential [21] (if the ion motion in the wake field is included, the wake potential is limited by $\varphi < \min[a_e^2, M/m]$). Thus, for $a_h \approx 1$ the ions gain an energy $\approx Mc^2$ during half a period of the wake wave and the ion motion in the wake of the laser pulse in an underdense plasma becomes relativistic. We note that this scaling is more favorable than the scaling, linear in the amplitude a_e, that would be obtained for a smooth long pulse interacting adiabatically with the plasma. This favorable scaling makes it possible to accelerate ions in the plasma to relativistic energies for amplitudes of the laser radiation much smaller than those for which the dimensionless amplitude calculated with the ion mass, $a_i = eE/M\omega c$, becomes of order 1, i.e., for which the ion quiver velocity equals the speed of light. This last amplitude corresponds to an intensity $I \approx 7\times 10^{24}$ W/cm^2 for a 1 μm laser in a hydrogen plasma.

The maximum energy that the particles can gain during the whole acceleration process when they interact resonantly with the wake can be estimated as $\approx e\varphi_m/(1 - v_{ph}/c)$ (see Ref. [22]), where $v_{ph} \approx c(1 - \omega^2/2\omega_{pe}^2)$ is the phase velocity of the wake wave. We see that in the petawatt regime the maximum energy does not depend on the pulse amplitude and is given by

$$\mathcal{E} \approx e\varphi_m(\omega/\omega_p)^2 \approx Mc^2(\omega/\omega_p)^2, \tag{2}$$

corresponding to $\approx$10–100 GeV in a plasma with density $n \approx (0.1 - 0.01) n_{\rm cr}$. As mentioned before these estimates have been obtained in the framework of a one-dimensional approximation. The effect of the transverse inhomogeneity of the laser-plasma interaction, due to the finite size of the laser beam, is expected to lower the amplitude of the wake field and the efficiency of the charged particle acceleration.

Similar estimates can be obtained for the case when the laser pulse interacts with an overdense plasma. We take the plasma to have the form of a thin slab of width l_s and assume that it is irradiated by a laser beam with amplitude a_e and radius $R \gg l_s$ at the focus. The electrons interacting with the laser light are expelled from their initial positions in the plasma slab. If the electron energy in the pulse field $\mathcal{E}_e = mc^2 a_e^2/2$ is large enough, they can overcome the attractive electric field due to charge separation. To move the electrons off (to distances larger than the laser spot size), the pulse amplitude must be such that $\mathcal{E}_e > \mathcal{E}_{\rm Coulomb}$, where the Coulomb energy is about $\mathcal{E}_{\rm Coulomb} \approx 2\pi e^2 n l_s R$, i.e.,

$$a_e > \left(\frac{l_s R}{d_e^2}\right)^{1/2} \equiv \left(\frac{4\pi\epsilon_0 R}{\lambda}\right)^{1/2}. \tag{3}$$

Here $d_e = c/\omega_{pe}$ is the collisionless skin depth and $\epsilon_0 = l_s\lambda/4\pi d_e^2$ the dimensionless parameter introduced in Ref. [23]. Later, the ions start to expand due to Coulomb repulsion (Coulomb explosion). They gain an energy of the order of $\mathcal{E}_{\rm Coulomb}$, which, assuming $\mathcal{E}_e \approx \mathcal{E}_{\rm Coulomb}$, can be rewritten as

$$\mathcal{E}_i \approx Mc^2\left(\frac{m}{M}\right) a_e^2 = Mc^2 a_h^2 \tag{4}$$

and is of the order of the ion rest mass when $a_h \approx 1$.

From the above estimates we expect that the laser acceleration of the ions in a plasma will result in a number of important effects that will make it possible to identify the mechanism of ion acceleration and that can be used for various applications such as the following. (1) Ion acceleration up to high energy values can shed light on the neutron production in overdense plasmas observed in [24]. (2) Ion acceleration opens up a way of producing laser induced nuclear reactions in a controlled way [25]. (3) The generation of GeV ions can be used for ion injection into conventional accelerators. (4) Compact sources of ions with energy in the range of several hundred MeV can be of interest for various applications in medicine [26,27].

The goal of the present paper is to analyze, with 2D PIC simulations, the mechanisms of ion acceleration by petawatt laser pulses in underdense and overdense plasmas in the nonadiabatic interaction regime. In Sec. II we study the interaction of such a laser pulse with a slab of underdense plasma and calculate the ion acceleration both inside the slab and in the plasma cloud that forms at the back of the slab after the laser pulse has drilled a hole through the slab. In Sec. III we study the interaction of a pulse in the petawatt power range with a slab of overdense plasma. We analyze the ion acceleration and collimation in two different cases: first from a flat plasma foil and then from a properly predeformed foil (converging lens).

II. INTERACTION OF A LASER PULSE WITH A SLAB OF UNDERDENSE PLASMA

First we investigate the interaction of a laser pulse with a slab of underdense plasma using 2D PIC fully relativistic simulations with ion to electron mass ratio $M/m = 1840$ ($\sqrt{M/m} = 43$). We consider a circularly polarized laser pulse with dimensionless amplitude $a_e = 50$. The pulse is Gaussian with full width $l_\perp = 10\lambda$ and length $l_\parallel = 20\lambda$. The plasma density is $n = 0.2025 n_{\rm cr}$ and corresponds to the ratio $\omega_{pe}/\omega = 0.45$. The length of the plasma slab is $L = 150\lambda$. It begins at $x = 0$ and is preceded by a vacuum region 5λ long and followed by a vacuum region 65λ long. The laser pulse is initialized outside the plasma in the vacuum region $x < 0$.

A. Ion acceleration inside the plasma slab

In Fig. 1 we present the (x,y) distribution of the electron (a) and ion (b) densities, of the x component of the electric field (c) and of the z component of the magnetic field (d) at

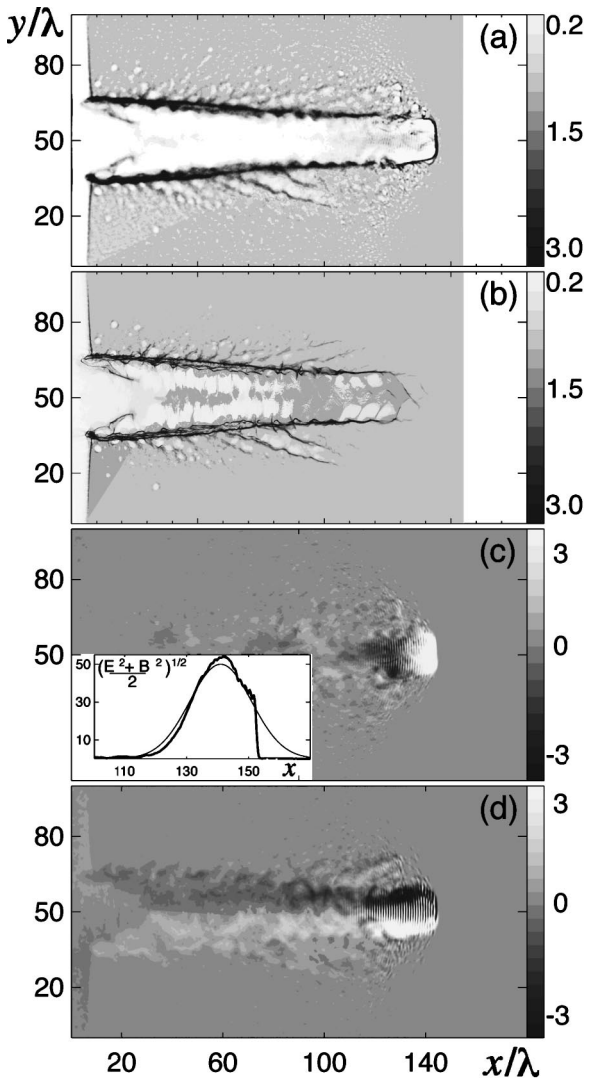

FIG. 1. The (x,y) distribution of the electron (a) and ion (b) densities, of the x component of the electric field (c), and of the z component of the magnetic field (d) at $t=170(2\pi/\omega)$. The thick line in the subframe in frame (c) shows $[(E^2+B^2)/2]^{1/2}$ on the pulse axis, while the thin line gives its initial distribution [shifted for comparison to the position of the pulse at $t=170(2\pi/\omega)$].

$t=170(2\pi/\omega)$. The laser pulse is focused in a relatively small region due to relativistic self-focusing and has developed a sharp front due to the effect of stimulated backward Raman scattering (SBRS). The formation of the sharp front, which is shown in the small subframe in (c), makes the interaction between the laser pulse and the plasma nonadiabatic and is responsible for the a_e^2 scaling of the electron and ion energies as mentioned in the Introduction. In Fig. 2 we show the phase planes (p_x,x) and (p_y,x) of electrons (a),(b) and ions (c),(d).

The main features exhibited by these simulations are these.

(1) A region with a strong electric field of opposite polarity is formed: electrons move first, pushed by the ponderomotive force of the laser pulse, and only later, because of their inertia, do ions start to move under the action of the electric field due to charge separation. As a result, a configuration propagating with the group velocity of the laser pulse is formed with an electric field that accelerates both electrons $(p_{xe}\approx 3600mc)$ and ions $(p_{xi}\approx 0.2Mc)$. The x distribution of the ion momentum along y has a structure that is not correlated with the position of the double layer.

(2) Behind this double polarity region the laser pulse expels both electrons and ions in the transverse direction. However, the channel behind the laser pulse is not totally evacuated as can be seen in Fig. 1. Indeed, the plasma moves predominantly outward in the radial direction, but at the same time an ''inverted'' corona mode of a hot, inward expanding plasma is formed. Reaching the channel axis, these hot plasma flows form a relatively dense plasma filament in the region $110\lambda<x<146\lambda$. The phenomenon of the inverted corona and of the formation of a hot filament inside the channel was discussed in Refs. [28,29] in the framework of the gas dynamics approximation. In the present case the situation is more complex: the inward expanding plasma is inhomogeneous in the direction along the channel and is formed by narrow jets, and the role of the particle collisions on the axis, leading to isotropization, is expected to be taken by the magnetic field. In addition a significant portion of the filament is made of the plasma that enters the channel through the front region of the channel. The electric current carried by the filament sustains the dipolar magnetic field which in turns focuses the plasma toward the axis.

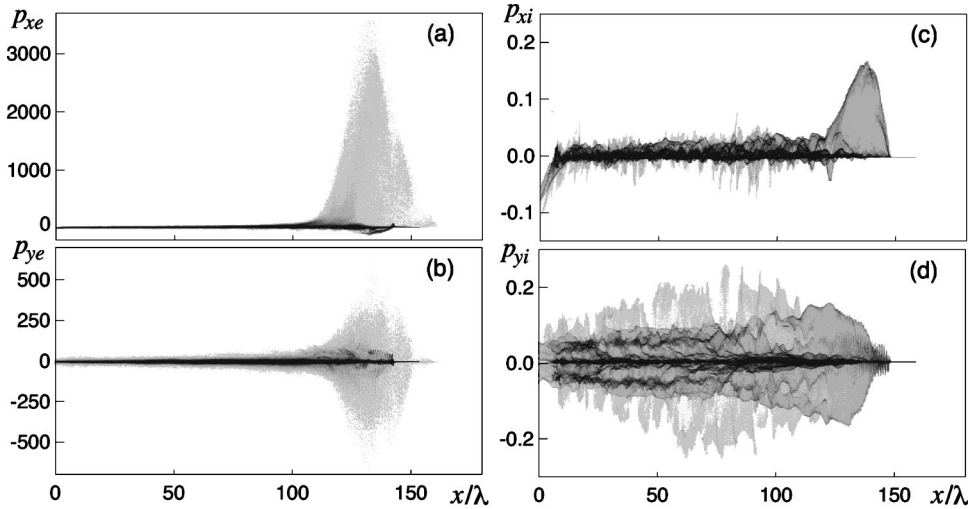

FIG. 2. The phase planes (p_{xe},x) and (p_{ye},x) of electrons (a),(b) and the phase planes (p_{xi},x) and (p_{yi},x) of ions (c),(d) at $t=170(2\pi/\omega)$.

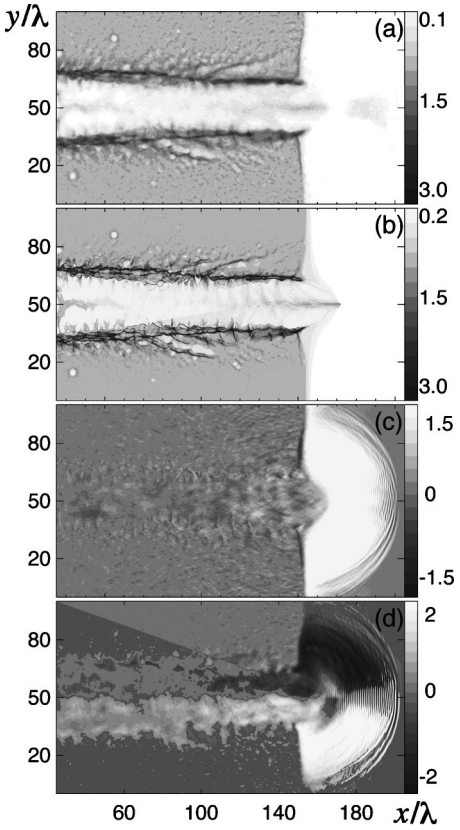

FIG. 3. The (x,y) distribution of the electron (a) and ion (b) densities, of the x component of the electric field (c), and of the z component of the magnetic field (d) at $t=230(2\pi/\omega)$.

B. Ion acceleration and collimation at the back of the plasma slab

After the laser pulse has bored through the plasma slab a high energy plasma cloud appears at the end of the channel at the back of the slab. Electrons expand in vacuum faster than ions and leave behind an ion cloud with a noncompensated electric charge.

Figure 3 gives the (x,y) distribution of the electron (a) and ion (b) densities, of the x component of the electric field (c), and of the z component of the magnetic field (d) at $t=230(2\pi/\omega)$, after the laser pulse has drilled a hole through the plasma slab, and Fig. 4 shows the corresponding phase planes (p_x,x) (a) and (p_x,y) (b) of electrons, and of ions (c,d). We see that the electron cloud expands into the vacuum region in the forward direction. The phase planes (p_x,x) of electrons (a) and of ions (c) show that the electron energy decreases while ions are accelerated up to relativistic energies $(p_{xi}>0.8Mc)$. We observe that, even at the quantitative level, the simplified estimates given in the Introduction are not too far from the values obtained with our PIC simulations. An important feature of these results is the ion collimation shown in the ion phase plane (p_{xi},y) in Fig. 4(d). This collimation can be explained by pinching in the self-generated magnetic field, which changes the polarity at the ion jet axis as shown by the slices of the ion (dash-dotted line) and electron (dashed line) densities and of the z component of the magnetic field (solid line) shown at $x=155.5$ in Fig. 5(a) and at $x=168.5$ in (b). We see that close to the channel end at $x=155.5$ the ion and electron densities in the filament are almost equal locally and the magnetic field is mainly produced by the electric current carried by the electrons. The magnetic field vanishes at the axis and changes its sign. At $x=168.5$ instead, near the filament axis, the ion density is much larger than the electron density. The dependence of the magnetic field on the y coordinate shows that inside the ion jet the magnetic field is produced by the electric current of the relativistic ions moving along the x direction.

C. Ion acceleration due to the Coulomb explosion

The mechanisms that accelerate the ions in the cloud at the back of the slab can be described by invoking the pull on the ions by the electrons that are expanding in the forward direction, and the inductive electric field generated by the fast change of the magnetic field during the expansion of the magnetized plasma cloud. These mechanisms work together with a continuous change from one to the other and provide an energy gain of the same order of magnitude. In order to obtain simple analytical estimates of the energy that the ions can acquire in the Coulomb explosion of the ion cloud, we adopt a simplified model that assumes spherical (cylindrical, planar) symmetry. We write the continuity equation for the ion density $N(r,t)$ as

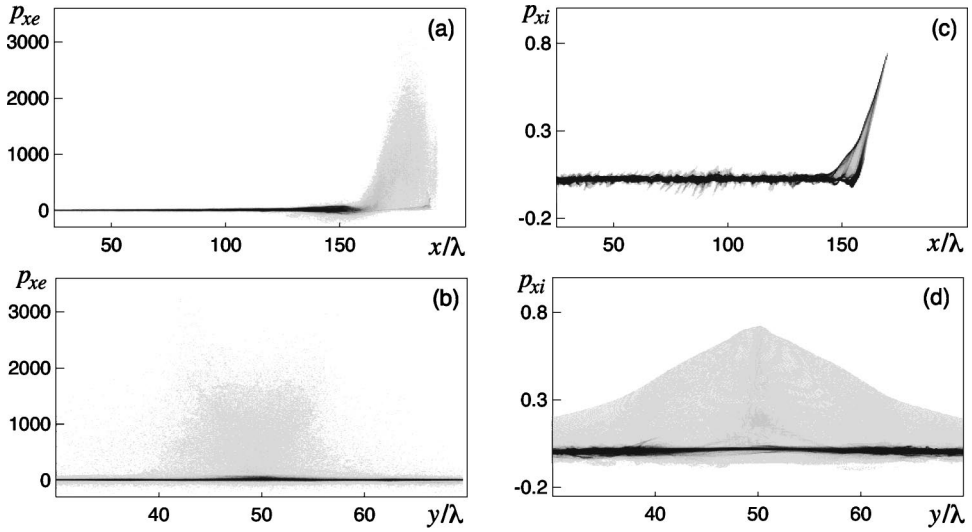

FIG. 4. The phase planes (p_{xe},x) and (p_{xe},y) of electrons (a),(b) and the phase planes (p_{xi},x) and (p_{xi},y) of ions (c),(d) at $t=230(2\pi/\omega)$.

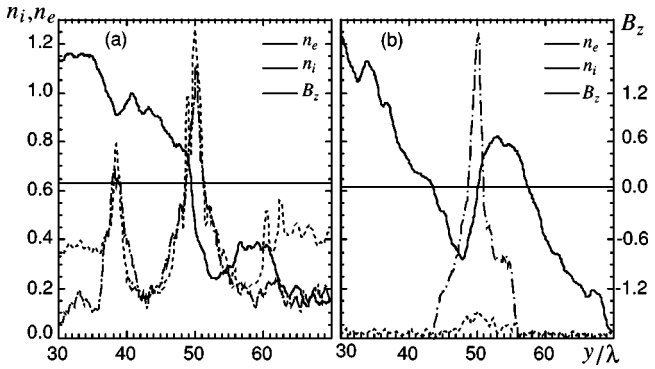

FIG. 5. Ion (dash-dotted line) and electron (dashed line) densities and the z component of the magnetic field (solid line) at $x=155.5$ in frame (a) and at $x=168.5$ in frame (b).

$$\partial_t N + r^{-\nu}\partial_r (r^\nu N v_r) = 0, \tag{5}$$

where $\nu = 0,1,2$ for planar, cylindrical, and spherical geometry, respectively. This equation must be solved with the boundary condition

$$r^\nu N v_r = J \quad \text{at } r = 0, \tag{6}$$

which corresponds to a point source of ions with intensity J at the origin and models the ion flux into the vacuum region from the channel drilled through the plasma slab. The equation of motion and Poisson equation read

$$\partial_t p_r + v_r \partial_r p_r = eE, \tag{7}$$

$$r^{-\nu}\partial_r (r^\nu E) = 4\pi e N. \tag{8}$$

Substituting the expression for the ion density obtained from Eq. (8) into Eq. (5), multiplying by r^ν, and integrating with respect to r, we obtain

$$\partial_t (r^\nu E) + v_r \partial_r (r^\nu E) = 4\pi e J. \tag{9}$$

Solving Eqs. (7) and (9), we obtain the equations for the characteristics $r(t)$ and $p(t)$ in the form

$$\partial_t p_r = eE, \tag{10}$$

$$\partial_t r = c\frac{p_r}{\sqrt{M^2c^2 + p_r^2}}, \tag{11}$$

$$\partial_t (r^\nu E) = 4\pi e J. \tag{12}$$

In the nonrelativistic limit, when $p_r \ll m_i c^2$, we find the following asymptotic dependence of the ion energy on r:

$$\mathcal{E}_i = \frac{(4\pi e^2 J m_i^{1/2})^{2/3}}{2^{1/3}} \times \begin{cases} (3r/2)^{4/3} & \text{for} \quad \nu = 0 \\ (9r/4)^{2/3} & \text{for} \quad \nu = 1 \\ (3\ln r/2)^{2/3} & \text{for} \quad \nu = 2. \end{cases} \tag{13}$$

For relativistic ion energies, $p_r \gg Mc$, $\partial_t r \approx c$, we obtain

$$\mathcal{E}_i = \frac{4\pi e^2 J}{c} \times \begin{cases} r^2/2 & \text{for} \quad \nu = 0 \\ r & \text{for} \quad \nu = 1 \\ \ln r & \text{for} \quad \nu = 2. \end{cases} \tag{14}$$

In the nonrelativistic case the ion flux J at the end of the channel can be estimated as $J = \pi R^2 N v_i$, with v_i the velocity of the ions at the channel end and R the channel radius. In the relativistic case we have $J = \pi R^2 N c$. Thus the typical ion energy is

$$\mathcal{E}_i \approx (\pi m c^2)^{2/3} \left(\frac{M v_i^2}{2}\right)^{1/3} \left(\frac{R}{d_e}\right)^{4/3} \text{ and}$$

$$\mathcal{E}_i \approx 4\pi N e^2 R^2 \approx m c^2 \left(\frac{R}{d_e}\right)^2, \tag{15}$$

in the nonrelativistic and in the relativistic case, respectively. In the simulations presented above the ratio of the channel radius to the collisionless skin depth is about 30, which gives $\mathcal{E}_i \approx 900 m c^2$, consistent with the value of the mean energy of fast ions seen in Fig. 4. Clearly, in a real configuration the Coulomb explosion is not spherically symmetric; nevertheless Eq. (15) gives the correct order of magnitude of the energy of the fast ions.

D. Ion acceleration due to the inductive electric field

During the expansion of the magnetized plasma cloud an inductive electric field is generated by the fast change of the magnetic field. As seen in Figs. 1, 3, and 5, the self-generated magnetic field vanishes at the axis and changes its sign in the upper and lower regions. When the electron-ion cloud leaves the channel it carries the magnetic field B frozen into the plasma at a distance larger than the collisionless skin depth. In the expanding plasma the magnetic field decreases and its value can be found from the conservation of the magnetic flux: $\Phi = \pi L^2 B = \text{const}$ where $L(t)$ is the cloud radius. At the beginning of the expansion, L is approximately equal to the channel radius R and B can be estimated from the expression for the self-generated magnetic field $B = 4\pi n e R$ obtained in [31]. The change of the magnetic field leads to the generation of the electric field $E = \dot{L}B/c = \dot{L}\Phi/\pi c L^2$ directed along the laser beam axis. This electric field accelerates the ions in the forward direction and slows down the electrons, which is similar to the acceleration mechanism that occurs during the process of magnetic field line reconnection (see [30]). A relativistic charged particle in the vicinity of the axis (where it is not magnetized) acquires an energy of the order of $\mathcal{E}_i \approx 4\pi n e^2 R^2$. This energy is of the order of the energy gain in the Coulomb explosion.

III. ION ACCELERATION IN A SLAB OF OVERDENSE PLASMA

In this section we first discuss the results of our 2D PIC simulations of the ion acceleration by an ultrarelativistic laser pulse in a flat slab of overdense plasma. Then, we consider a properly predeformed plasma slab (''convergent lens''), which makes it possible to optimize the collimation of the accelerated ion beam at the back of the slab. The size of the simulation region is $12.4\times 15\lambda^2$. The boundary conditions are periodic in the y direction for the particles and the electromagnetic fields. The boundaries in the x direction are absorbing for the electromagnetic waves while the particles are reflected with the thermal velocity. The number of grid

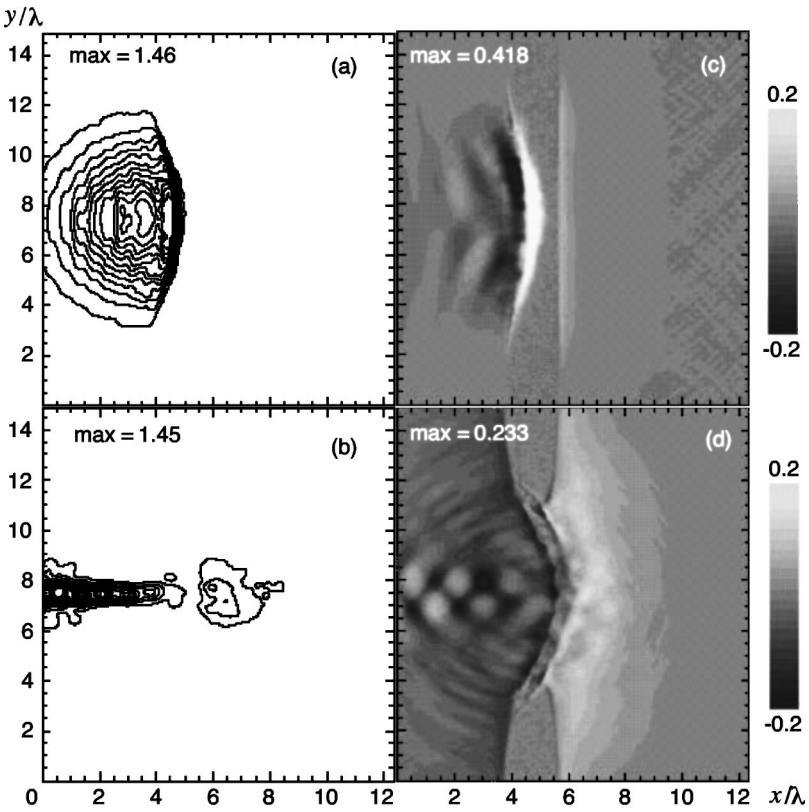

FIG. 6. Electromagnetic energy density (a) and (b) and E_x component of the electric field (c) and (d). [Frames (a) and (c) present the configuration at $t=9(2\pi/\omega)$, and frames (b) and (d) correspond to $t=15(2\pi/\omega)$.] The electromagnetic energy density is normalized to the peak value in the incident laser pulse. The contour levels vary from 0.1 to 1.2 with the interval 0.1. The electric field is nomalized to the laser field E_{y0}.

points and particles in the simulations is 850×1024 and 7.2×10^6.

In the first case a plasma slab (a thin foil) is localized initially at $5\lambda<x<7\lambda$. In the second case a foil of thickness 2λ is predeformed in its central part in the shape of the parabola given, for $x<6\lambda$, by the formula $x=4\lambda+0.32(y-7.5\lambda)^2/\lambda$. In both cases the maximum plasma density is $n=30n_{\rm cr}$ and the plasma consists of protons (ion mass $M=1840m$) and electrons with initial electron and ion temperatures equal to 800 eV.

We expect that in the case of the predeformed foil the high absorption of an obliquely incident *p*-polarized pulse and the additional focusing of the transmitted light will lead to a more effective ion acceleration than in the case of the flat foil configuration. An ultraintense *p*-polarized laser pulse is initiated at the left hand side boundary. The pulse has a Gaussian profile in both the longitudinal and the transverse directions, its length and spot size (its width) are 5.5λ and 5λ, respectively. The normalized amplitude of the incident pulse is equal to $a_e=89$, and is larger than $\sqrt{M/m}\simeq43$. Thus we expect that the ions are accelerated up to extremely high energies. For a 1 μm laser, this intensity corresponds to 1.6×10^{22} W/cm^2 and the pulse length to 18 fs. Such pulse parameters are within the reach of the technological developments that can be expected to occur in the next few years [32].

For the chosen parameters of the laser pulse and of the plasma, the dimensionless parameter $\epsilon_0=\omega_{pe}^2 l_s/2\omega c$ [see Eq. (3)] is equal to 180. The normalized laser amplitude $a_e=89$ is smaller than ϵ_0. In this case, according to Ref. [23] the foil is not transparent to the laser radiation and only a relatively small portion of the radiation can be transmitted through the foil.

A. Interaction of the laser pulse with a flat thin foil

The results of our simulations of the interaction of the laser pulse with the flat foil are shown in Fig. 6. Frames (a) and (c) correspond to $t=9(2\pi/\omega)$ and frames (b) and (d) correspond to $t=15(2\pi/\omega)$. Frames (a) and (b) show the distribution of the electromagnetic energy density and frames (c) and (d) show the x component of the electric field in the (x,y) plane. We see the deformation of the foil surface under the ponderomotive pressure that pushes the electrons in the

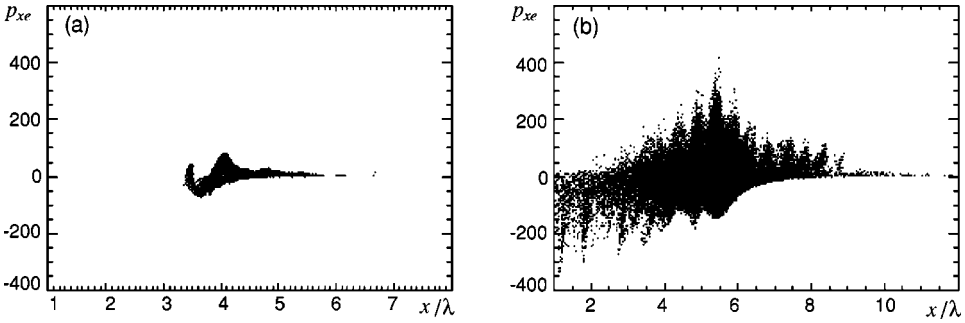

FIG. 7. The phase plane (p_{xe},x) of electrons with energy above 1.5 MeV at $t=9(2\pi/\omega)$ (a) and at $t=15(2\pi/\omega)$ (b).

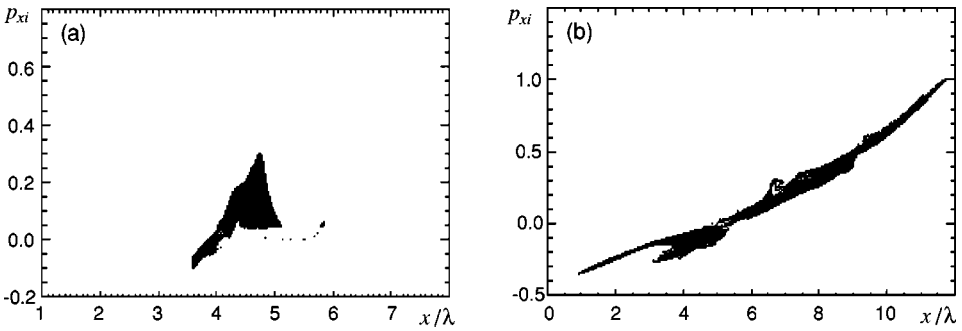

FIG. 8. The phase plane of ions (p_{xi},x) at $t=9(2\pi/\omega)$ (a) and at $t=15(2\pi/\omega)$ (b).

forward direction. The electric charge separation leads to the generation of a strong electrostatic field as shown in frames (b) and (d). A relatively small fraction of pulse is transmitted: the fractions of the transmitted and of the reflected energies are about 6.1% and 42.2%, respectively. An important feature exhibited by Fig. 6 is the strong focusing of the radiation reflected in the backward direction, as found in Ref. [23]. The transverse size of the reflected beam spot is close to one wavelength. This backward focusing of the electromagnetic radiation is a nonlinear effect caused by the deformation of the critical surface under the light pressure. We analyze this deformation of the target induced by the radiation and the resulting backward self-focusing in the so called snow plough model. In this approximation the critical surface moves inside a thick plasma as

$$\xi(t)=\frac{E}{\sqrt{4\pi nM}}t=a_e\left(\frac{\omega}{\omega_{pe}}\right)\sqrt{\frac{m}{M}}ct, \tag{16}$$

and, in the case of a thin foil of width l_s, as

$$\xi(t)=a_e^2\left(\frac{\omega}{\omega_{pe}}\right)^2\frac{m}{M}\frac{c^2t^2}{l_s}. \tag{17}$$

Expanding the laser pulse amplitude near its axis as $a_e \approx a_0[1-y^2/(2l_\perp^2)]$, where $l_\perp$ is the pulse transverse inhomogeneity scale, we find that the foil gets deformed into a parabolic shape given by

$$x=\xi_0(t)[1-\beta y^2/(2l_\perp^2)]. \tag{18}$$

For a thick plasma $\beta=1$ and $\xi_0(t)$ is given by Eq. (16) with $a=a_0$, while for a thin foil $\beta=2$ and $\xi_0(t)$ is given by Eq. (17). The radiation reflected from the mirror is focused at the distance $x_f=l_\perp^2/2\beta\xi_0(t)$, which approaches the plasma-vacuum interface as the deformation of the mirror grows.

Charged particles are accelerated very effectively both in the forward and in the backward directions. In Fig. 7 the phase plane of the electrons with energy above 1.5 MeV is shown at $t=9(2\pi/\omega)$ in frame (a), and at $t=15(2\pi/\omega)$ in frame (b). We see in frame (a) that the electrons are accelerated in the forward direction by the ponderomotive force

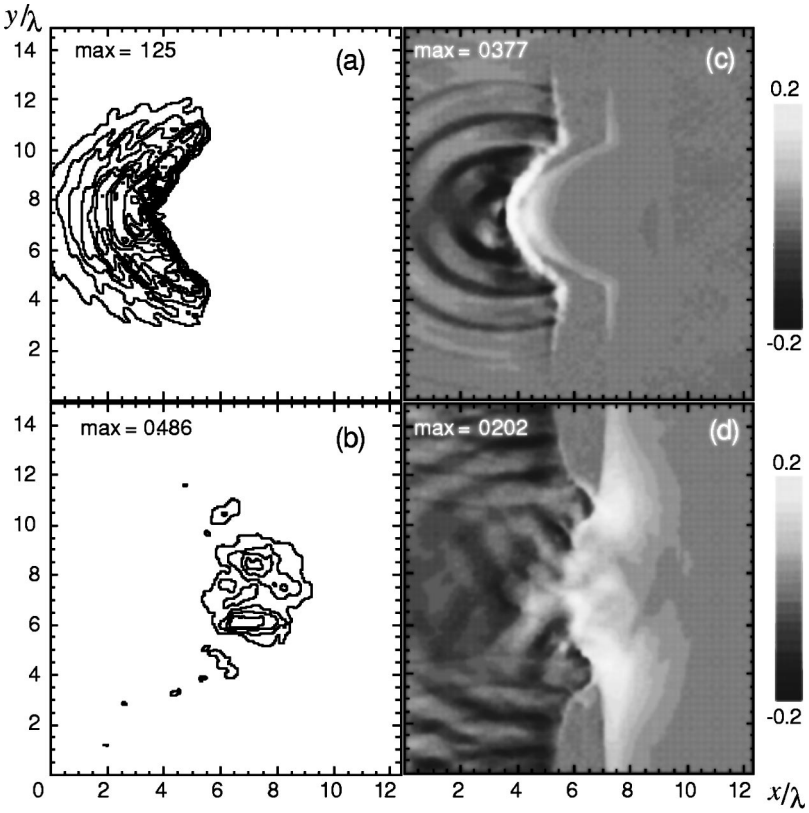

FIG. 9. The same as in Fig. 6 in the case of the interaction of the laser pulse with a predeformed foil.

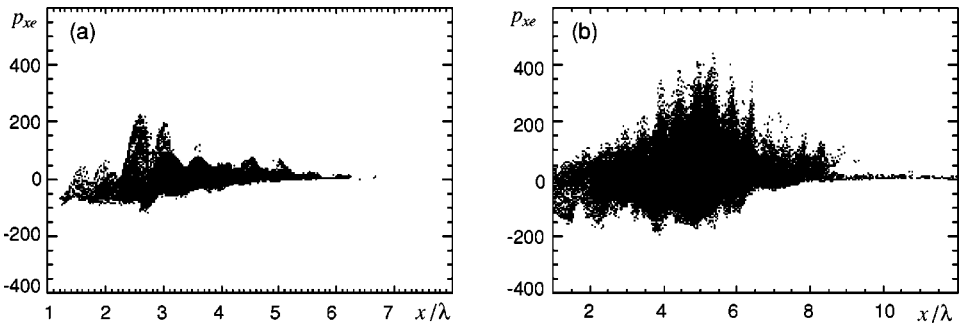

FIG. 10. The phase plane (p_{xe},x) of electrons with energy above 1.5 MeV at $t=9(2\pi/\omega)$ (a) and at $t=15(2\pi/\omega)$ (b) in the case of the predeformed foil.

and are extracted in the backward direction due to ''vacuum heating'' [34,35]. In Fig. 7(b) we see that the electrons are accelerated in the forward direction twice per laser period due to the $\mathbf{v}\times\mathbf{B}$ force [36,37] and the energetic electrons are accelerated in the backward direction once per laser period as observed in Refs. [38,39].

The phase plane of the fast ions is shown in Fig. 8 at $t=9(2\pi/\omega)$ in frame (a) and at $t=15(2\pi/\omega)$ in frame (b). We see that the ions are accelerated both in the backward direction, as discussed in Ref. [35], and in the forward direction. The forward ion acceleration is predominant. The maximum momentum reached by the ions is $p_{xi}/Mc\sim 1$, which corresponds to the GeV energy range. Also, in this case the acceleration mechanism must be attributed to the Coulomb explosion which gives a final ion energy of the order of $\mathcal{E}_{\mathrm{Coulomb}}\approx 4\pi e^2 n l_s l_\perp = 4\pi^2 mc^2(\omega_{pe}/\omega)^2(l_s l_\perp/\lambda^2)$. For the parameters of the simulations $\mathcal{E}_{\mathrm{Coulomb}}\approx Mc^2$, i.e., ≈ 1 GeV.

B. Ion acceleration from a predeformed foil

The deformation of the flat foil induced by the pulse causes a strong focusing of the back reflected radiation. Similarly, a strong collimation of the particles accelerated in the forward direction can be expected when using a predeformed foil with a curvature opposite to that which would be induced by the radiation (converging lens). The foil is assumed to be initially deformed in the shape of a parabola, as described as the beginning of Sec. III and shown in Fig. 9.

We notice that converging plasma flows, formed under irradiation of a semicylindrical foil, were investigated experimentally for moderate laser powers in Ref. [33]. It was shown that a hot plasma filament is formed at the axis. The theoretical description of this process was developed in Ref. [28]. In the present paper we study this process in the relativistic range of plasma parameters where a jet of relativistic ions is formed at the axis instead of a high density filament of hot plasma.

In Fig. 9 frames (a) and (c) correspond to $t=9(2\pi/\omega)$ and frames (b) and (d) correspond to $t=15(2\pi/\omega)$. Frames (a) and (b) show the distribution of the electromagnetic energy density and frames (c) and (d) show the x component of the electric field in the (x,y) plane. Since the target is initially deformed, the laser pulse is incident obliquely in the regions outside the center. This causes a high absorption of the laser radiation with the fractions of the reflected and transmitted laser light equal to 16.26% and 12.26%. The energy of the reflected radiation is three times smaller than in the case of an initially flat foil. In Fig. 10 we see that the electrons are accelerated more effectively, as compared to the case of the flat foil. The plasma heating up to relativistic energies reduces the refraction index inside the foil, and, as a result, the transmission of the light eventually increases [40]. Figure 11 shows the phase plane of the fast ions. A sharp peak in the (p_x,x) plane appears at $t=9(2\pi/\omega)$, as seen in Fig. 11(a). This is a significant difference from the case of the flat foil presented in Fig. 8. The peak is formed due to the focusing of the converging ion flows toward the axis and to the expansion of the ion cloud in the forward direction. At $t=15(2\pi/\omega)$, as seen in Fig. 11(b), the ion energy is relativistic and the acceleration is predominantly in the forward direction. The maximum ion momentum reaches $p_{xi}/Mc\sim 1.2$.

C. Electromagnetic filamentation and ion jets in the plasma cloud

A the comparison of the time evolution of the electron and ion mean kinetic energies for the flat and for the predeformed foil is shown in Fig. 12. The solid lines correspond to the flat foil and the dotted lines correspond to the deformed foil. In the case of the deformed foil, the energy gain of both electrons and ions is higher than in the case of the flat foil, but not significantly so. A more significant difference can be seen in the spatial distribution of the fast ions shown in Figs.

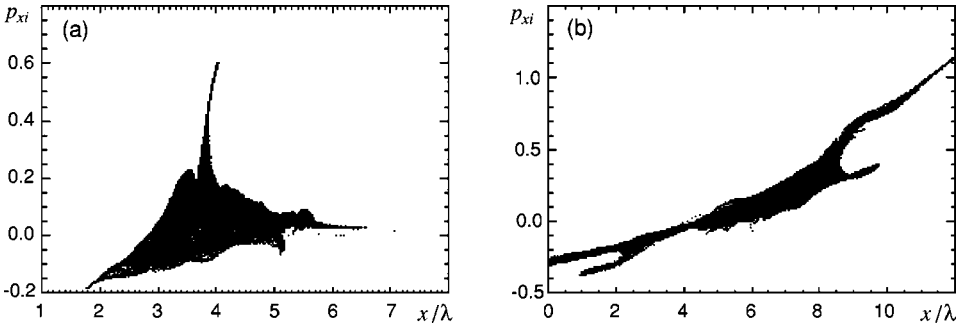

FIG. 11. The phase plane of ions (p_{xi},x) at $t=9(2\pi/\omega)$ (a) and at $t=15(2\pi/\omega)$ (b) in the case of the predeformed foil.

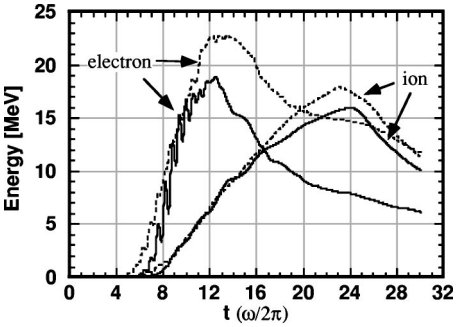

FIG. 12. The electron and ion average energies versus time in the cases of the flat and the predeformed foil.

13 and 14. In Fig. 13 we present the energy density of electrons (a) and ions (b) in the (x,y) plane at $t=15(2\pi/\omega)$ in the case of the flat foil. In frames (c) and (d) we present the same distributions in the case of the deformed foil and in frame (e) the energy density of ions at $t=21(2\pi/\omega)$.

In Fig. 14 we present the z component of the magnetic field (a), the x component of the electric field (b), the electromagnetic energy density of the laser radiation (c), the energy density of the ions (d), the density of the electric charge (n_i-n_e) (e), and the plot of the quasistatic magnetic field and the ion energy density at $x=4.65$ versus the y coordinate at $t=12(2\pi/\omega)$ (f) in the case of the deformed foil. In Figs. 13(a) and 13(b) we see that the distribution of the electrons expanding in the forward direction inside the plasma is much less structured than the ion distribution. The ion density shows very clear filaments with scale length of the order of the laser wavelength. In order to explain these structures we invoke the electromagnetic filamentation instability. Since the mean energy of the electrons in the expanding plasma is approximately equal to the ion energy, as seen in Fig. 12, electrons move faster than ions. As is well known, a plasma with a net relative motion between electrons and ions is unstable. This instability is similar to the electron filamentation instability considered in Ref. [41]. It is easy to show that the growth rate of this filamentation instability is

$$\Gamma = Q\omega_{pi}/\sqrt{Q^2+\omega_{pe}^2/c^2\gamma^3}, \tag{19}$$

where Q is the wave number of the perturbations and $\gamma=\mathcal{E}_e/mc^2$ is the electron Lorentz factor. For our simulation parameters we obtain that the scale length $2\pi/Q \approx 2\pi c\gamma^{3/2}/\omega_{pe}$, below which the growth rate becomes approximately constant, is of the order of the laser wavelength and that the characteristic time scale of the instability is approximately $2\pi/\omega_{pi}\approx 8(2\pi/\omega)$.

The filamentation of the ion component is also present in the plasma cloud moving in the backward direction in the case of the deformed foil [see Figs. 13(e), 13(f), 14(d) and 14(e)]. The electromagnetic nature of this instability is apparent from the correlation between the ion filaments and the regions of reverse polarity of the magnetic field [see Fig. 14(a)]. In the case of the deformed foil the ions moving in the forward direction form a single filament in the shape of a jet. Inside this filament the electric charge neutrality is broken, as seen in Fig. 14(e). However, the repulsion in the transverse direction due to the electric force is partially balanced by the magnetic part of the Lorentz force. The pinching does not confine the ions in the longitudinal direction: they expand and gain energy. In Fig. 14(f) the quasistatic magnetic field and the ion energy density at $x=4.65$ versus the y coordinate at $t=12(2\pi/\omega)$ are shown. The quasistatic magnetic field is approximately ten times smaller than the magnetic field in the laser pulse, i.e., approximately 300 MG. The transverse size of the ion jet is equal to 0.2λ, much smaller than the laser wavelength. The magnetic pinching inside the jet and, in the case of the predeformed plasma foil, the converging plasma flow lead to an increase of the ion density. In Fig. 15 we show the ion density evolution at the laser beam axis. On the vertical axis the ion density is measured in units of the critical plasma density. In frame (a) the ion density is presented in the case of a flat foil. We see that at $t=9(2\pi/\omega)$ the ion density is about three

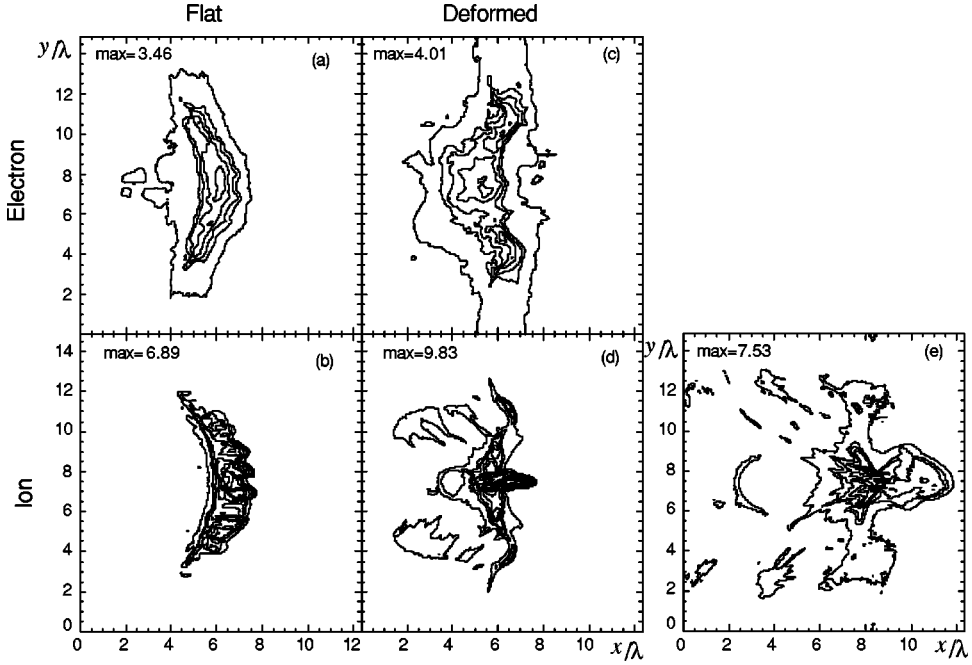

FIG. 13. The energy density of electrons (a) and of ions (b) in the (x,y) plane at $t=15(2\pi/\omega)$ in the case of the flat foil. In frames (c) and (d) the same distributions in the case of the predeformed foil and in frame (e) the energy density of ions at $t=21(2\pi/\omega)$.

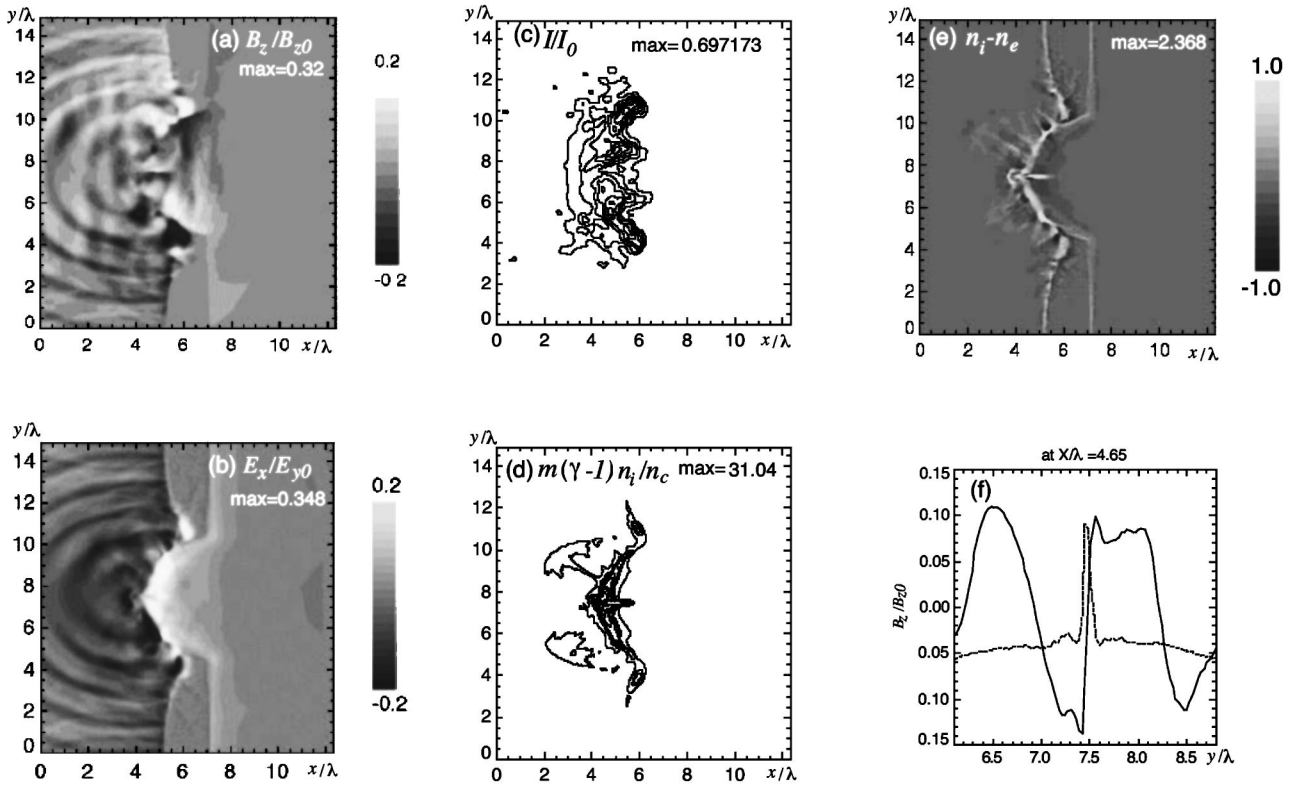

FIG. 14. Laser pulse interaction with the predeformed foil. The z component of the magnetic field (a), the x component of the electric field (b), the electromagnetic energy density of the laser radiation (c), the energy density of the ions (d), the density of the electric charge (n_i-n_e) (e), and the plot of the quasistatic magnetic field and the ion energy density at $x=4.65$ versus the y coordinate at $t=12(2\pi/\omega)$ (f).

times higher than the initial density in the foil. Later the density decreases, but remains well above critical density at $t=18(2\pi/\omega)$. The ion compression in the case of the deformed foil is considerably higher. In frame (b) we see that at $t=6(2\pi/\omega)$ the compression rate equals about 7. At $t=18(2\pi/\omega)$ the ion density in the jet is only twice smaller than the initial density in the foil and is equal to $15n_{\mathrm{cr}}$, which corresponds to a density of relativistic ions of the order of 10^{22} cm^{-3}.

IV. CONCLUSION

With the help of 2D3V PIC simulations, we have investigated the ion acceleration during the interaction of petawatt laser pulses with underdense and overdense plasma slabs. The laser-slab interaction is accompanied by a broad range of physical processes, among which we mention the backward self-focusing of the laser light reflected by the foil deformed by the radiation. Ion acceleration is the main concern of this paper. In underdense plasmas we emphasize the formation of an electric double layer moving with relativistic velocity at the head of the plasma channel drilled by the laser pulse and the formation of a plasma filament on the channel axis. In the radial direction the ions are accelerated predominantly toward the channel walls up to energies corresponding to the value of the ponderomotive potential. At the channel head ions are accelerated in the forward direction by the electric field of a moving double layer. The situation changes dramatically when the laser pulse reaches the end of the slab. In this case, the plasma filament begins to expand at the end of the channel. High energy electrons expand faster and the ions form a well collimated relativistically moving jet, confined in the transverse direction by the pinching in the self-generated magnetic field. The ions in the jet expand in the longitudinal direction because the electric charge is not compensated inside the jet. For the parameters that are character-

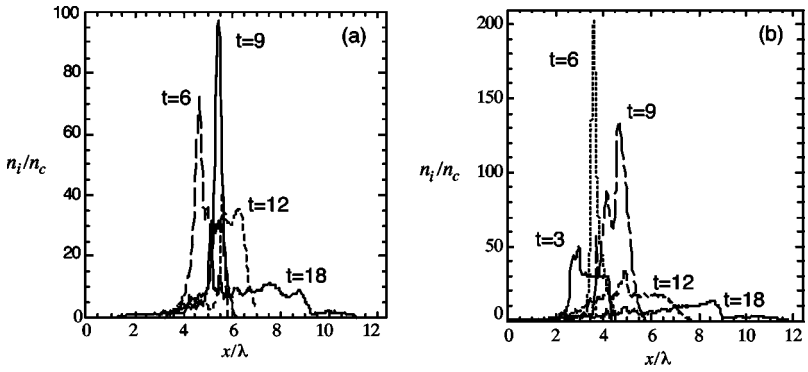

FIG. 15. Ion density evolution at the laser beam axis in the case of the flat (a) and the predeformed foil (b). The ion density is measured in units of the critical plasma density.

istic of the interaction of a petawatt laser pulse with a near-critical plasma this ''anisotropic Coulomb explosion'' accelerates ions up to relativistic energies. We have shown that the mechanism of anisotropic Coulomb explosion is also at work in the case of the interaction of a petawatt laser with a thin slab of overdense plasma and accelerates ions up to relativistic energies. The electromagnetic filamentation instability leads to magnetic pinching in the transverse direction and to jet formation. A very well collimated ion jet can be obtained using a properly predeformed plasma foil. With a parabolic foil we have obtained an ion jet with a transverse size much smaller than 1 μm and a density of the order of 10^{22} cm^{-3}.

ACKNOWLEDGMENTS

The authors acknowledge helpful discussions with V. Yu. Bychenkov, A. V. Gordeev, H. Hojo, J. Koga, A. Maksimchuk, K. Nakajima, P. Norreys, and V. T. Tikhonchuk. This work was supported in part by the INFM Parallel Computing Initiative. S.B. and N.N. recognize support from the Science and Technology Agency of Japan.

[1] J.D. Kmetec *et al.*, Phys. Rev. Lett. **68**, 1527 (1992).
[2] W.L. Kruer and S.C. Wilks, Plasma Phys. Controlled Fusion **34**, 2061 (1992).
[3] J. Denavit, Phys. Rev. Lett. **69**, 3052 (1992).
[4] D. Gordon *et al.*, Phys. Rev. Lett. **80**, 2133 (1998).
[5] F.N. Beg *et al.*, Phys. Plasmas **4**, 447 (1997).
[6] S.-Y. Chen, M. Krishnan, A. Maksimchuk, R. Wagner, and D. Umstadter, Phys. Plasmas **6**, 4739 (1999).
[7] C. Gahn *et al.*, Phys. Rev. Lett. **83**, 4772 (1999).
[8] A.G. Zhidkov *et al.*, Phys. Rev. E **60**, 3273 (1999).
[9] P.A. Norreys *et al.*, Phys. Plasmas **6**, 2150 (1999).
[10] G.S. Sarkisov *et al.*, Phys. Rev. E **59**, 7042 (1999).
[11] K. Krushelnik *et al.*, Phys. Rev. Lett. **82**, 2095 (1999).
[12] L. Disdier, J.-P. Garçonnet, G. Malka, and J.-L. Miguel, Phys. Rev. Lett. **82**, 1454 (1999).
[13] G.I. Moore *et al.*, Phys. Rev. E **61**, 788 (2000).
[14] K.W.D. Ledigham *et al.*, Phys. Rev. Lett. **84**, 899 (2000); T.E. Cowan *et al.*, *ibid.* **84**, 903 (2000).
[15] G.S. Sarkisov, V.Yu. Bychenkov, V.T. Tikhonchuk, A. Maksimchuk, S.Y. Chen, R. Wagner, G. Mourou, and D. Umstadter, Pis'ma Zh. Éksp. Teor. Fiz. **66**, 787 (1987) [JETP Lett. **66**, 828 (1997)].
[16] N.H. Burnett and G.D. Enright, IEEE J. Quantum Electron. **26**, 1797 (1990).
[17] S.V. Bulanov, F. Califano, G.I. Dudnikova, T.Zh. Esirkepov, F.F. Kamenets, T.V. Liseikina, N.M. Naumova, F. Pegoraro, and V.A. Vshivkov, Plasma Phys. Rep. **25**, 468 (1999).
[18] T.Zh. Esirkepov *et al.*, JETP Lett. **70**, 82 (1999).
[19] S. Miyamoto, S. Kato, K. Mima, H. Takamaru, R. Horiuchi, and T. Sato, J. Plasma Fusion Res. **73**, 343 (1997).
[20] S.V. Bulanov, I.N. Inovenkov, V.I. Kirsanov, N.M. Naumova, and A.S. Sakharov, Phys. Fluids B **4**, 1935 (1992); C.D. Decker, W.B. Mori, and T.K. Katsouleas, Phys. Rev. E **50**, R3338 (1994); K.-C. Tseng, W.B. Mori, and C.D. Decker, Phys. Rev. Lett. **76**, 3332 (1996); S.V. Bulanov, F. Pegoraro, and A.M. Pukhov, *ibid.* **74**, 710 (1995).
[21] S.V. Bulanov, V.I. Kirsanov, and A.S. Sakharov, Pis'ma Zh. Éksp. Teor. Fiz. **50**, 156 (1989) [JETP Lett. **50**, 175 (1989)]; V.I. Berezhiani and I.G. Murusidze, Phys. Lett. A **148**, 338 (1990); P. Sprangle, E. Esarey, and A. Ting, Phys. Rev. Lett. **64**, 2011 (1990).
[22] T. Tajima and J. Dawson, Phys. Rev. Lett. **43**, 267 (1979).
[23] V.A. Vshivkov, N.M. Naumova, F. Pegoraro, and S.V. Bulanov, Phys. Plasmas **5**, 2727 (1998).
[24] F.N. Beg *et al.*, Phys. Plasmas **4**, 447 (1997); P.A. Norreys *et al.*, Plasma Phys. Controlled Fusion **40**, 175 (1998).
[25] V.Yu. Bychenkov, V.T. Tikhonchuk, and S.V. Tolokonnikov, JETP **88**, 1137 (1999).
[26] U. Amaldi and M. Silari, *The Tera Project and the Center for Oncological Hadrontherapy* (INFN-LNF Divisione Ricerca, Frascati, 1995).
[27] V.S. Khoroshkov and E.I. Minakova, Eur. J. Phys. **19**, 523 (1998).
[28] G.A. Askar'yan, S.V. Bulanov, and I.V. Sokolov, Plasma Phys. Rep. **25**, 549 (1999).
[29] S.Y. Chen, G.S. Sarkisov, A. Maksimchuk, and D. Umstadter, Phys. Rev. Lett. **80**, 2610 (1998).
[30] V.S. Berezinsky, S.V. Bulanov, V.A. Dogiel, V.L. Ginzburg, and V.S. Ptuskin, *Astrophysics of Cosmic Rays* (North Holland, Amsterdam, 1990); S.V. Bulanov and P.V. Sasorov, Astron. Zh. **52**, 763 (1975) [Sov. Astron. **19**, 464 (1975)]; S.V. Bulanov and F. Cap, *ibid.* **65**, 837 (1988) [**32**, 436 (1988)].
[31] G.A. Askar'yan, S.V. Bulanov, F. Pegoraro, and A.M. Pukhov, Pis'ma Zh. Éksp. Teor. Fiz. **60**, 240 (1994) [JETP Lett. **60**, 251 (1994)].
[32] G.A. Mourou, C.P.J. Barty, and M.D. Perry, Phys. Today **51** (1), 22 (1998).
[33] G.A. Askar'yan, M.G. Korolev, and L.L. Yakushkin, Pis'ma Zh. Éksp. Teor. Fiz. **57**, 164 (1993) [JETP Lett. **57**, 167 (1993)].
[34] F. Brunel, Phys. Rev. Lett. **59**, 52 (1987).
[35] S.V. Bulanov, N.M. Naumova, and F. Pegoraro, Phys. Plasmas **1**, 745 (1994).
[36] S.C. Wilks, W.L. Kruer, M. Tabak, and A.B. Langdon, Phys. Rev. Lett. **69**, 1383 (1992).
[37] Y. Sentoku, K. Mima, T. Taguchi, S. Miyamoto, and Y. Kishimoto, Phys. Plasmas **5**, 4366 (1998).
[38] H. Ruhl, Y. Sentoku, K. Mima, K.A. Tanaka, and R. Kodama, Phys. Rev. Lett. **82**, 743 (1999).
[39] Y. Sentoku, H. Ruhl, K. Mima, R. Kodama, K.A. Tanaka, and Y. Kishimoto, Phys. Plasmas **6**, 2855 (1999).
[40] H. Ruhl, A. Macchi, P. Mulser, F. Cornolti, and S. Hain, Phys. Rev. Lett. **82**, 2095 (1999).
[41] F. Califano, F. Pegoraro, S.V. Bulanov, and A. Mangeney, Phys. Rev. E **57**, 7048 (1998); F. Califano, R. Prandi, F. Pegoraro, and S.V. Bulanov, *ibid.* **58**, 7837 (1998); Y. Kazimura, J.-I. Sakai, and S.V. Bulanov, J. Phys. Soc. Jpn. **68**, 3271 (1999); Y. Sentoku, K. Mima, S.-I. Kojima, and H. Ruhl, Phys. Plasmas **7**, 689 (2000).